Cathepsin G–Mediated Activation of Pro–Matrix Metalloproteinase 9 at the Tumor-Bone Interface Promotes Transforming Growth Factor-β Signaling and Bone Destruction

Thomas J. Wilson, Kalyan C. Nannuru, and Rakesh K. Singh

Department of Pathology and Microbiology, University of Nebraska Medical Center, Omaha, Nebraska

Abstract

Increased transforming growth factor-β (TGF-β) signaling has been observed at the tumor-bone interface of mammary tumor–induced osteolytic lesions despite no observed transcriptional up-regulation of TGF-β. To this point, the mechanism for enhanced TGF-β signaling remains unclear. The bulk of TGF-β that is released at the tumor-bone interface is in an inactive form secondary to association with β-latency–associated protein and latency TGF-β binding protein. We hypothesized that the observed increase in TGF-β signaling is due to increased cathepsin G–dependent, matrix metalloproteinase 9 (MMP9)–mediated activation of latent TGF-β. MMP9 is capable of activating latent TGF-β, and we observed that decreased production of MMP9 was associated with reduced TGF-β signaling. Similar to TGF-β, MMP9 is released in an inactive form and requires proteolytic activation. We showed that cathepsin G, which we have previously shown to be up-regulated at the tumor-bone interface, is capable of activating pro-MMP9. Inhibition of cathepsin G *in vivo* significantly reduced MMP9 activity, increased the ratio of latent TGF-β to active TGF-β, and reduced the level of TGF-β signaling. Our proposed model based on these results is that cathepsin G is up-regulated through tumor-stromal interactions and activates pro-MMP9, active MMP9 cleaves and releases active TGF-β, and active TGF-β can then promote tumor growth and enhance osteoclast activation and subsequent bone resorption. Thus, for the first time, we have identified cathepsin G and MMP9 as proteases involved in enhanced TGF-β signaling at the tumor-bone interface of mammary tumor–induced osteolytic lesions and have identified these proteases as potential therapeutic targets. (Mol Cancer Res 2009;7(8):1224–33)

Received 1/19/09; revised 4/16/09; accepted 5/8/09; published OnlineFirst 8/11/09. The costs of publication of this article were defrayed in part by the payment of page charges. This article must therefore be hereby marked *advertisement* in accordance with 18 U.S.C. Section 1734 solely to indicate this fact.

Note: T.J. Wilson is a Howard Hughes Medical Institute Research Training Fellows.

Requests for reprints: Rakesh K. Singh, Department of Pathology and Microbiology, University of Nebraska Medical Center, 985900 Nebraska Medical Center, Omaha, NE 68198-5900. Phone: 402-559-9949; Fax: 402-559-5900. E-mail: rsingh@unmc.edu

doi:10.1158/1541-7786.MCR-09-0028

Introduction

Breast cancer affects approximately one in eight women in the United States (1). The majority of morbidity and mortality occurs as breast cancer cells form distant metastases, making the progression from primary breast tumor to metastasis an ominous sign in the progression of the disease. Common sites for metastasis include the bone, lung, liver, and brain, with bone being the most common site distant to the lymph nodes (1). The establishment of distant colonies in the bone microenvironment yields osteolytic lesions leading to anemia, intractable bone pain, hypercalcemia, and increased risk of pathologic fracture. This constellation of consequences both significantly reduces the quality of life for the patient as well as dramatically increases the likelihood of mortality (2). Thus, understanding the molecular mechanisms involved in the bidirectional communication that occurs between mammary tumor cells and bone stromal cells is vitally important for designing new therapeutic interventions.

As malignant breast cancer cells enter the bone microenvironment, a vicious cycle occurs that promotes both tumor growth and osteolysis (3). One signaling axis that is particularly important is the receptor activator of NF-κB (RANK)-RANK ligand (RANKL) signaling axis (2, 4-9). The activation of osteoclasts by this signaling axis leads to bone degradation, which releases growth factors previously sequestered in the bone matrix that promote further tumor growth. One such sequestered factor that is released is transforming growth factor-β (TGF-β; ref. 2).

TGF-β has been shown to have a variety of effects in the bone microenvironment, including chemoattraction of tumor cells, serving as a mitogen for tumor cells, and enhancing osteolysis (10). The effect of TGF-β on osteolysis is mediated by both RANKL-dependent and RANKL-independent mechanisms. Increased TGF-β signaling has been shown at the tumor-bone interface of mammary tumor–induced osteolytic lesions despite no observed transcriptional up-regulation (11). Inhibition of TGF-β signaling using a neutralizing antibody or TGF-βRI kinase inhibitor significantly reduced osteolysis, suggesting the importance of this signaling axis. *In vitro* data suggest that TGF-β enhances RANKL signaling, as treatment of RAW 264.7 cells (osteoclast precursors) with TGF-β did not enhance osteoclast differentiation or activation but treatment of these cells with TGF-β plus RANKL showed significantly enhanced osteoclast differentiation and activation compared with RANKL treatment alone (11).

In addition to working synergistically with RANKL to increase osteoclast differentiation and activation, enhanced

TGF-β signaling also results in increased production of parathyroid hormone–related peptide (PTHrP) by tumor cells. PTHrP functions in a similar manner to parathyroid hormone by enhancing RANKL expression by osteoblasts, ultimately leading to increased osteoclast activation and bone resorption. Inhibition of TGF-β signaling significantly reduced PTHrP production and correspondingly reduced tumor-induced osteolysis. Conversely, transfection of the mammary tumor cell line MDA-MB-231 with cDNA for PTHrP, causing constitutive expression of PTHrP, significantly enhanced tumor-induced osteolysis (12).

As previously mentioned, enhanced TGF-β signaling has been shown at the tumor-bone interface (11). However, TGF-β transcriptional levels have never been shown to be increased and no mechanism for the observed increase in TGF-β signaling has been described. TGF-β that is released from the bone matrix is predominantly in an inactive form due to association with TGF-β latency-associated protein (β-LAP; refs. 10, 13) and latent TGF-β binding protein (LTBP). A variety of latent, high molecular weight complexes are secreted with the predominant form being ~220 kDa and composed of a TGF-β homodimer, β-LAP, and LTBP (14, 15). To a lesser extent, a smaller, ~75 kDa complex of a TGF-β homodimer and β-LAP is also secreted (16). The active form is composed of a TGF-β homodimer, which is ~25 kDa and is free of association with LTBP and β-LAP (14, 15). Thus, with the majority of secreted TGF-β being in a latent form, one potential mechanism for enhanced TGF-β signaling is enhanced cleavage and activation of TGF-β.

Both matrix metalloproteinase (MMP) 2 and MMP9 are capable of proteolytically activating TGF-β (10). We have previously reported that MMP9 is up-regulated at the tumor-bone interface (3); however, MMP9 is also secreted as a zymogen necessitating activation in order for it to be functional. We have also previously reported that cathepsin G is up-regulated at the tumor-bone interface (3). Cathepsin G has previously been shown to be capable of activating pro-MMP2, a gelatinase related to MMP9 (17). In this report, we sought to delineate the mechanism of enhanced TGF-β signaling at the tumor-bone interface of mammary tumor–induced osteolytic lesions and hypothesized that up-regulation of cathepsin G may lead to increased activation of MMP9 and subsequently increased release of active TGF-β. We report that inhibition of MMP9 expression at the tumor-bone interface significantly reduced TGF-β signaling, suggesting that MMP9 may be responsible for activation of latent TGF-β. We also report that cathepsin G is capable of cleaving and activating pro-MMP9 and that inhibition of cathepsin G *in vivo* reduced MMP9 activity at the tumor-bone interface, increased the ratio of latent TGF-β to active TGF-β, and reduced TGF-β signaling.

Results

TGF-β Signaling Is Enhanced in Mammary Tumor–Induced Osteolytic Lesions

Cl66 cells implanted onto the calvaria of BALB/c mice generated osteolytic lesions that mimic changes associated with human breast cancer. We evaluated TGF-β signaling at both the tumor-bone interface and tumor alone area. The tumor-bone interface showed a significantly higher phosphorylated Smad-2 (P-Smad-2) staining index compared with the tumor alone area (Fig. 1A and B). This suggested that TGF-β signaling is enhanced at the tumor-bone interface.

MMP9 Activity Is Increased at the Tumor-Bone Interface

MMP9 belongs to the gelatinase group of MMPs. Thus, to evaluate MMP9 activity at the tumor-bone interface, gelatin zymography was done. Areas of clearing against a stained background at ~110 kDa represent areas of MMP9 gelatinolytic activity. MMP9 activity was increased at the tumor-bone interface compared with the tumor alone area in all three mice, with no observable MMP9 activity in the tumor alone area of two of the three tumors (Fig. 1C and D). No MMP2 activity was observed at either the tumor-bone interface or tumor alone area.

Inhibition of RANKL Signaling Reduces MMP9 Activity and TGF-β Signaling

RANKL signaling has previously been shown to increase MMP9 expression (18, 19). We first attempted to confirm these findings. We treated the murine monocyte/macrophage cell line RAW 264.7 (osteoclast precursors) with soluble RANKL (sRANKL) and evaluated MMP9 expression. RAW 264.7 cells treated with sRANKL showed a progressive increase in MMP9 mRNA expression and gelatinolytic activity that was maximal 7 days after treatment (Fig. 2A). MMP9 expression was correlated with activated osteoclast number (data not shown).

Because RANKL signaling leads to increased expression of MMP9, mice were treated with RANKL-antisense oligonucleotides (ASO) to reduce MMP9 expression at the tumor-bone interface. We first evaluated mRNA expression of MMP9 and MMP2, another member of the gelatinase family of MMPs. MMP9 mRNA expression was significantly reduced in RANKL-ASO–treated mice (Fig. 2B), whereas MMP2 expression was similar between control-treated and RANKL-ASO–treated mice (Fig. 2C).

We then evaluated MMP9 activity using gelatin zymography to confirm reduced MMP9 activity in RANKL-ASO–treated mice. The gelatin zymogram showed significantly decreased MMP9 activity (less gelatinolytic activity at 110 kDa) in the RANKL-ASO–treated mice (Fig. 3A and B). No MMP2 gelatinolytic activity was observed in either RANKL-ASO–treated or control-treated mice.

TGF-β signaling was then evaluated at the tumor-bone interface of RANKL-ASO and control ASO–treated mice. We evaluated TGF-β signaling using immunohistochemistry for P-Smad-2 (20). We observed a significant decrease in the P-Smad-2 staining index and thus TGF-β signaling at the tumor-bone interface of mice with MMP9 expression reduced by RANKL-ASO treatment (Fig. 3C and D).

Cathepsin G Activates Pro-MMP9

Next, we tested the ability of cathepsin G to cleave and activate pro-MMP9. We purchased commercially available MMP9 that was mainly in zymogen form with minimal amounts of active MMP9 per the manufacturer's product data sheet. The native product containing mainly pro-MMP9 showed minimal ability to cleave a chromogenic MMP substrate (Fig. 4A). Cathepsin G showed no ability to cleave the chromogenic MMP substrate (Fig. 4A). MMP9 preincubated

with cathepsin G showed significantly increased ability to cleave the MMP substrate, showing that cathepsin G is activating pro-MMP9 (Fig. 4A).

To further confirm the ability of cathepsin G to activate pro-MMP9, we used protein samples from the tumor alone area of control ASO–treated mice and did gelatin zymography with these samples. We observed minimal MMP9 activity in these samples (Fig. 4B). However, when these samples were preincubated with cathepsin G, we observed a significant increase in MMP9 gelatinolytic activity (Fig. 4B). This shows that pro-MMP9 was present in the tumor alone area and was activated by cathepsin G.

Inhibition of Cathepsin G Reduces MMP9 Activity and TGF-β Signaling

Mice were treated with *N*-tosyl-L-phenylalanine chloromethyl ketone (TPCK) to inhibit cathepsin G activity. We then evaluated MMP9 activity at the tumor-bone interface of TPCK- and control-treated mice. TPCK treatment significantly reduced MMP9 activity at the tumor-bone interface compared with control-treated mice (Fig. 4C and D).

We then evaluated TGF-β signaling at the tumor-bone interface by evaluating P-Smad-2 staining. The P-Smad-2 staining index was significantly decreased in TPCK-treated animals showing reduced TGF-β signaling in these animals (Fig. 5A and B).

Finally, we compared the bone destruction index, MMP9 gelatinolytic activity, and P-Smad-2 staining index for each individual mouse in the TPCK- and control-treated groups. We found both the MMP9 gelatinolytic activity and P-Smad-2 staining index to be highly correlated with the bone destruction index in individual mice. The Pearson correlation coefficient between the bone destruction index and MMP9 gelatinolytic

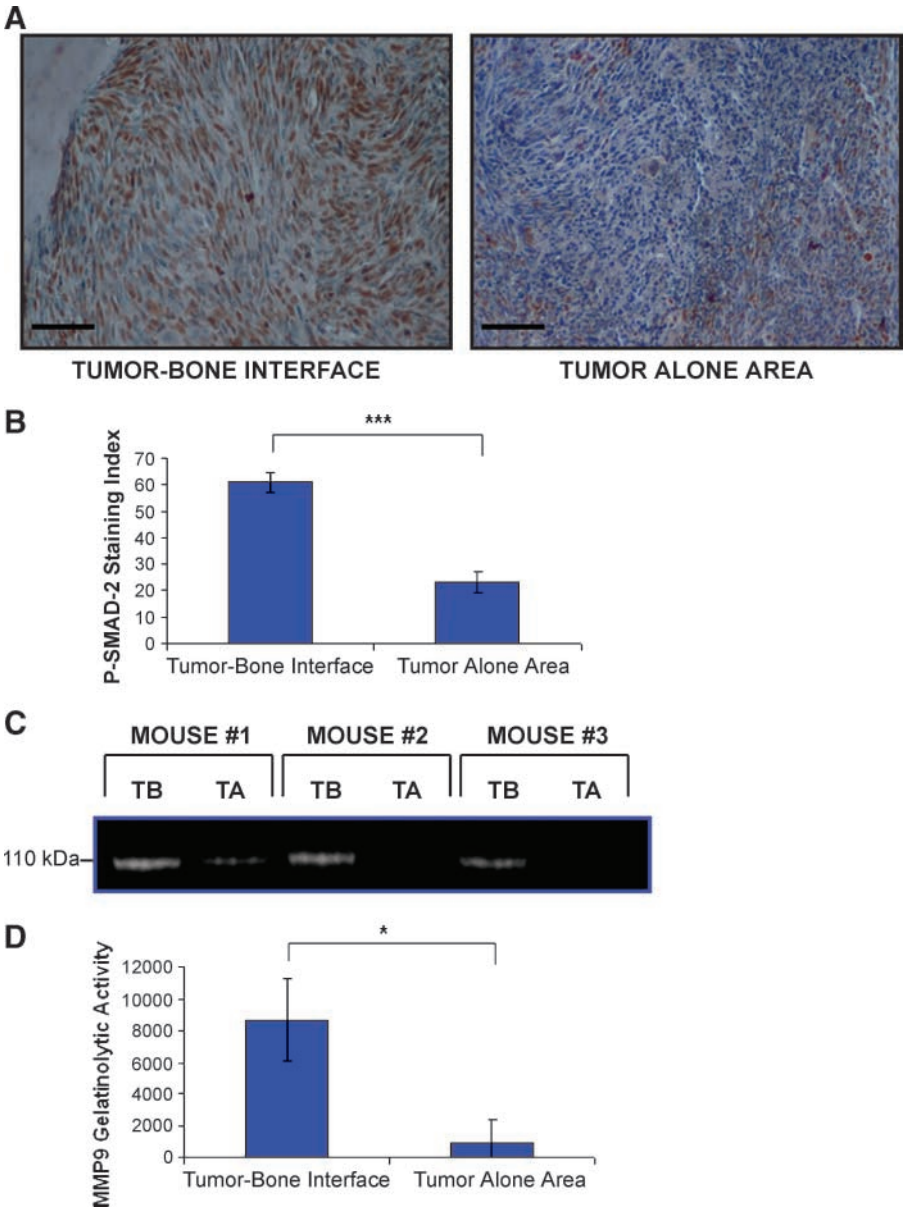

FIGURE 1. TGF-β signaling and MMP9 activity at the tumor-bone interface. **A** and **B.** The P-Smad-2 staining index was significantly higher at the tumor-bone interface compared with the tumor alone area in Cl66-induced osteolytic lesions. Bars, SD. Scale bars, 0.01 mm. ***, $P < 0.001$. **C** and **D.** Gelatinolytic activity at ~110 kDa representing MMP9 was significantly increased at the tumor-bone interface compared with the tumor alone area of mammary tumor–induced osteolytic lesions. Bars, SD. *, $P < 0.05$.

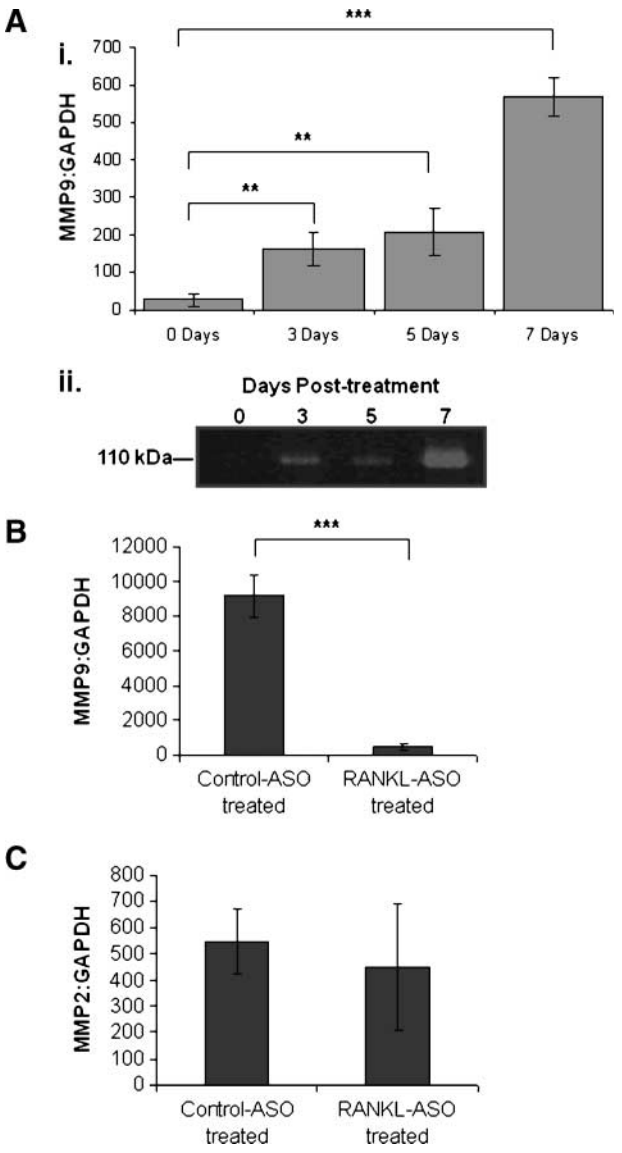

FIGURE 2. RANKL-ASOs reduce MMP9 expression but do not affect MMP2 expression. **A.** i, treatment of the murine monocyte/macrophage cell line RAW 264.7 with sRANKL enhanced expression of MMP9. Maximal expression of MMP9 was observed 7 d after treatment. Bars, SD. *, $P < 0.05$; **, $P < 0.01$; ***, $P < 0.001$. ii, MMP9 gelatinolytic activity similarly increased to a peak at 7 d after treatment. **B.** qRT-PCR showed that RANKL-ASO treatment significantly reduced mRNA expression of MMP9 at the tumor-bone interface. **C.** RANKL-ASO–treated mice showed no difference in MMP2 mRNA expression at the tumor-bone interface compared with control ASO–treated mice.

activity was 0.916, whereas the Pearson correlation coefficient between the bone destruction index and the P-Smad-2 staining index was 0.920 (Fig. 5C). MMP9 activity was also positively correlated with the P-Smad-2 staining index with a Pearson correlation coefficient of 0.960.

Inhibition of Cathepsin G Reduces Active TGF-β at the Tumor-Bone Interface

We used Western blot analysis to compare the relative proportions of latent TGF-β and active TGF-β at the tumor-bone interface of control- and TPCK-treated mice. An antibody to TGF-β was used to label both the latent TGF-β complex (~220 kDa) and the active TGF-β homodimer (~25 kDa). β-Actin was used to normalize the samples. TPCK-treated animals showed a significantly higher ratio of latent to active TGF-β compared with control-treated animals (Fig. 6A and B).

Discussion

In this report, we delineated one mechanism of enhanced TGF-β signaling at the tumor-bone interface of mammary tumor–induced osteolytic lesions. TGF-β in latent form due to association with β-LAP and LTBP is found sequestered in the bone matrix (10, 13). Mammary tumor–induced bone degradation allows release of this sequestered growth factor. Increased TGF-β signaling has been observed at the tumor-bone interface of mammary tumor–induced osteolytic lesions, which plays a pivotal role in enhancing osteolysis by both RANKL-dependent and RANKL-independent mechanisms (11, 12). Despite observing increased TGF-β signaling, transcriptional up-regulation of TGF-β has never been shown. Understanding the mechanism by which TGF-β signaling is increased could potentially reveal therapeutic targets in breast cancer–induced osteolytic lesions. Here, we provide data to support that inhibition of cathepsin G at the tumor-bone interface may lead to decreased activation of MMP9, subsequently resulting in reduced release of active TGF-β.

We first showed that TGF-β signaling is, in fact, increased at the tumor-bone interface in our model (11). MMP2 and MMP9 have both been previously shown to be capable of cleaving and activating TGF-β. Thus, up-regulation of either of these proteins at the tumor-bone interface would represent a potential mechanism by which TGF-β signaling could be enhanced. We have previously reported that MMP9 is up-regulated at the tumor-bone interface of mammary tumor–induced osteolytic lesions (3). We did not observe up-regulation of MMP2 (3). We confirmed that there is increased MMP9 activity using gelatin zymography. We observed increased MMP9 gelatinolytic activity at the tumor-bone interface. Importantly, we did not observe any MMP2 gelatinolytic activity at either the tumor-bone interface or tumor alone area. This allowed us to focus on the role of MMP9. If up-regulation of MMP9 is the mechanism by which TGF-β signaling is enhanced, we would expect that if MMP9 expression or activity was reduced at the tumor-bone interface, TGF-β signaling would similarly be decreased.

The RANKL-RANK signaling axis is important at the tumor-bone interface in the differentiation and activation of osteoclasts (3, 9, 21-24). Osteoclasts are major producers of MMP9 (25-29). Because RANKL has been shown to increase MMP9 expression, we treated mice with RANKL-ASOs to reduce the production of MMP9 at the tumor-bone interface (18, 19). We confirmed that RANKL-ASO–treated mice had less MMP9 mRNA expression. MMP2 expression was unchanged by RANKL-ASO treatment. Furthermore, we confirmed that RANKL-ASO–treated mice show reduced MMP9 activity using gelatin zymography, which showed significantly reduced MMP9 activity at the tumor-bone interface compared with control ASO–treated mice. No MMP2 gelatinolytic activity was observed.

We then sought to test whether enhanced MMP9 expression contributes to increased TGF-β signaling. If MMP9 cleavage and activation of TGF-β are important for enhanced signaling, with reduced MMP9 activity, we would expect to see reduced TGF-β signaling. The P-Smad-2 staining index, a measure of TGF-β signaling, was significantly reduced in mice depleted of MMP9 activity by RANKL-ASO treatment. This suggests that MMP9 may be responsible for enhanced TGF-β signaling via increased production of the active 25-kDa TGF-β homodimer. Because MMP2 expression was unchanged, this cannot be attributed to alteration in MMP2 activity.

MMP9, however, is secreted as a zymogen. Consequently, an additional protease is required to activate pro-MMP9 to allow it to activate TGF-β. Cathepsin G has previously been shown to be capable of activating pro-MMP2, a member of the gelatinase family of MMPs similar to MMP9 (17). However, to our knowledge, cathepsin G has never been shown to activate pro-MMP9. If cathepsin G was capable of activating pro-MMP9, it would represent a potential and likely mechanism for enhanced TGF-β signaling whereby cathepsin G activates pro-MMP9 and active MMP9 activates TGF-β. Thus, we sought to determine if cathepsin G is capable of activating pro-MMP9. We purchased commercially available MMP9, which was primarily in the zymogen form with a small amount of active MMP9. We tested this enzyme against a chromogenic substrate and found minimal cleavage of the substrate. We also tested cathepsin G against the same substrate, and as expected, it was not capable of cleaving the substrate. We did,

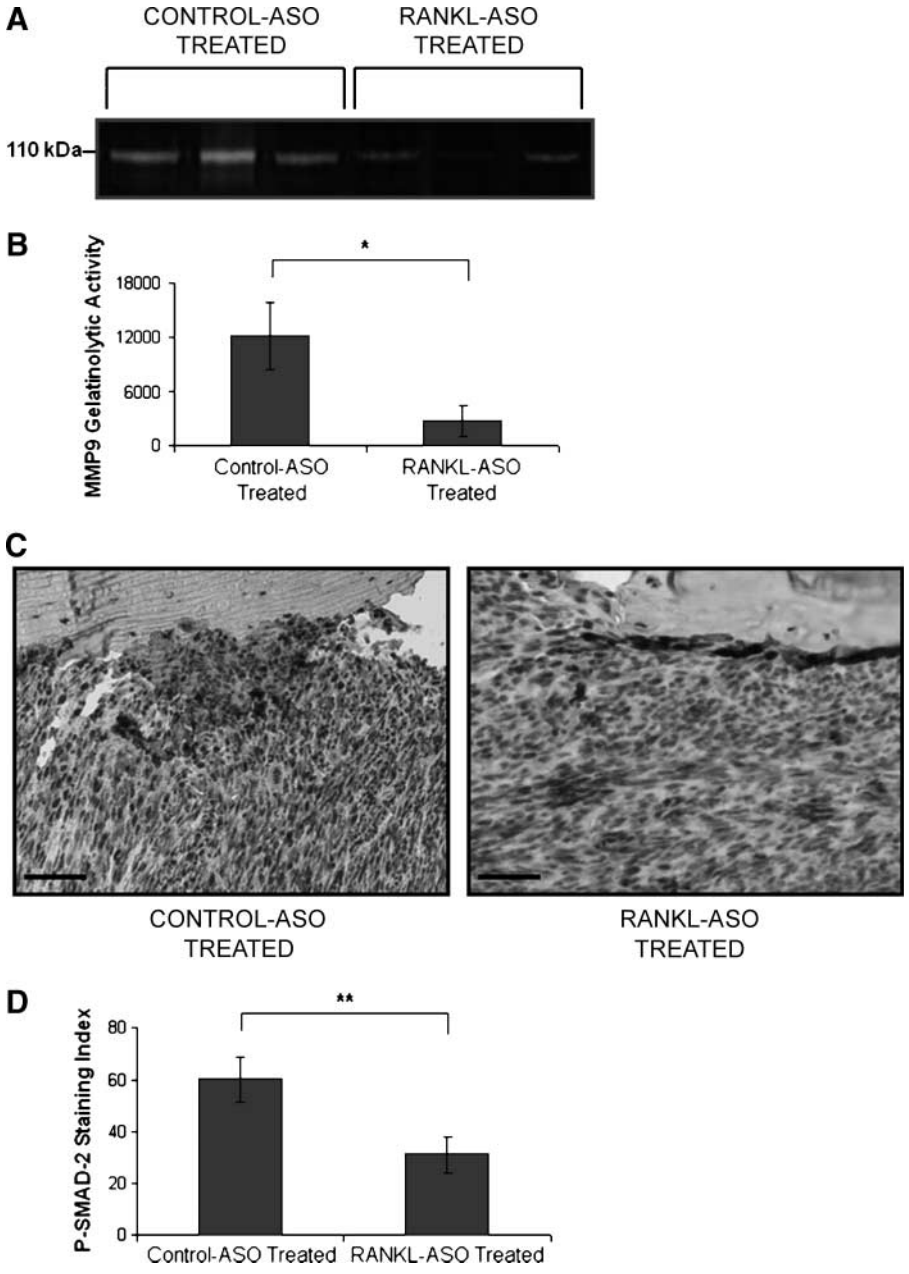

FIGURE 3. MMP9 activity and TGF-β signaling are decreased at the tumor-bone interface in RANKL-ASO–treated mice. **A** and **B.** MMP9 gelatinolytic activity (110 kDa) was significantly reduced at the tumor-bone interface of RANKL-ASO–treated mice compared with control ASO–treated mice. Bars, SD. *, $P < 0.05$. **C** and **D.** The P-Smad-2 staining index was significantly reduced at the tumor-bone interface of RANKL-ASO–treated mice compared with control ASO–treated mice. Bars, SD. Scale bars, 0.01 mm. **, $P < 0.01$.

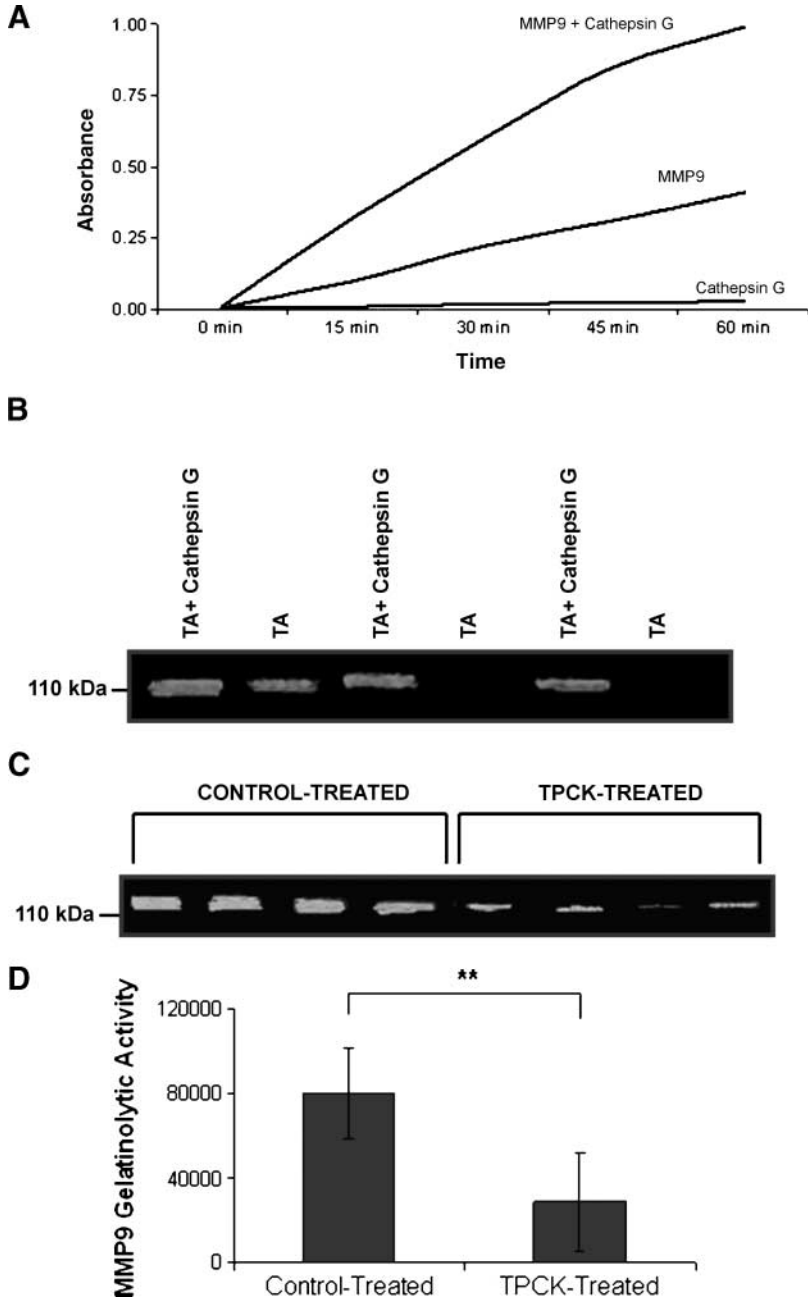

FIGURE 4. Cathepsin G activates pro-MMP9 *in vitro* and *in vivo*. **A.** A commercially available mixture of pro-MMP9 and MMP9 that was predominantly pro-MMP9 showed minimal ability to cleave a chromogenic MMP substrate. Cathepsin G showed no ability to cleave the same substrate. Pro-MMP9/MMP9 preincubated with cathepsin G showed increased ability to cleave the chromogenic MMP substrate, suggesting that cathepsin G is capable of activating pro-MMP9. **B.** Samples from the tumor alone area of mammary tumor–induced osteolytic lesions showed minimal MMP9 gelatinolytic activity. Samples from the tumor alone area that were preincubated with cathepsin G showed enhanced MMP9 gelatinolytic activity, suggesting that pro-MMP9 was present and activated by cathepsin G. **C** and **D.** Treatment with TPCK, an inhibitor of cathepsin G, significantly reduced MMP9 gelatinolytic activity at the tumor-bone interface compared with control (DMSO)–treated mice. Bars, SD. **, $P < 0.01$.

however, observe that pro-MMP9 preincubated with cathepsin G showed markedly increased cleavage of the substrate, suggesting that cathepsin G is capable of activating pro-MMP9.

To further confirm that cathepsin G can cleave and activate pro-MMP9, we examined the gelatinolytic activity of MMP9 using samples from the tumor alone area. We used these samples because we have shown them to have minimal MMP9 gelatinolytic activity. We also preincubated these samples with cathepsin G, assuming that if pro-MMP9 was present in the sample and cathepsin G was capable of activating it, we would see enhanced gelatinolytic activity in the samples preincubated with cathepsin G. In fact, we did observe enhanced gelatinolytic activity, further confirming that cathepsin G is capable of activating pro-MMP9.

With this potential mechanism, we sought to test this *in vivo* by inhibiting cathepsin G. The assumption of this experiment was that if cathepsin G is responsible for activating pro-MMP9, which when active enhances TGF-β signaling, then inhibition of cathepsin G should decrease both MMP9 activity at the tumor-bone interface and subsequently decrease TGF-β signaling.

TPCK was used to inhibit cathepsin G *in vivo* (3). TPCK-treated animals exhibited significantly reduced MMP9 activity at the tumor-bone interface compared with control-treated animals. Furthermore, TPCK-treated animals showed markedly

reduced TGF-β signaling at the tumor-bone interface as shown by a reduced P-Smad-2 staining index. This shows that this mechanism likely occurs *in vivo*. We observed a strong correlation between both MMP9 activity and the bone destruction index and the P-Smad-2 staining index and the bone destruction index in individual mice.

Latent TGF-β exists primarily as a complex of TGF-β, β-LAP, and LTBP that is ~220 kDa. The active form of TGF-β is a homodimer that is ~25 kDa. We used Western blot analysis to compare the relative proportion of latent TGF-β and active TGF-β in control- and TPCK-treated mice. TPCK-treated animals had a significantly higher amount of latent TGF-β compared with active TGF-β at the tumor-bone interface. This shows that inhibition of cathepsin G results in less proteolytic activation of latent TGF-β. Based on the rest of our results, we propose that this is due to reduced activation of pro-MMP9.

TGF-β signaling enhances osteolysis as well as promotes tumor growth and angiogenesis. For the first time, we have identified one mechanism that contributes to enhance TGF-β signaling at the tumor-bone interface of mammary tumor–induced osteolytic lesions. In other pathologic systems, cathepsin G–mediated activation of pro-MMP2 and subsequent MMP2-mediated activation of TGF-β may be important. The lack of MMP2 up-regulation at the tumor-bone interface, lack of observable MMP2 gelatinolytic activity, and lack of down-regulation of MMP2 in RANKL-ASO–treated mice argue against this mechanism being important for breast cancer–induced bone lesions. We have identified cathepsin G, MMP9, and TGF-β as potential targets for therapeutic intervention that would have the potential to reduce mammary tumor–induced osteolysis. We have previously shown that inhibition of cathepsin G *in vivo* significantly reduces osteolysis by decreasing the generation of sRANKL (3). However, these data suggest that the observed reduction in osteolysis may be due not only to reduced sRANKL generation but also to reduced pro-MMP9 activation and subsequent TGF-β signaling.

Materials and Methods

Animal Model and Tissue Preparation

A murine bone invasion model was used as previously described (3). Cl66 tumor cells (1×10^5), a murine breast

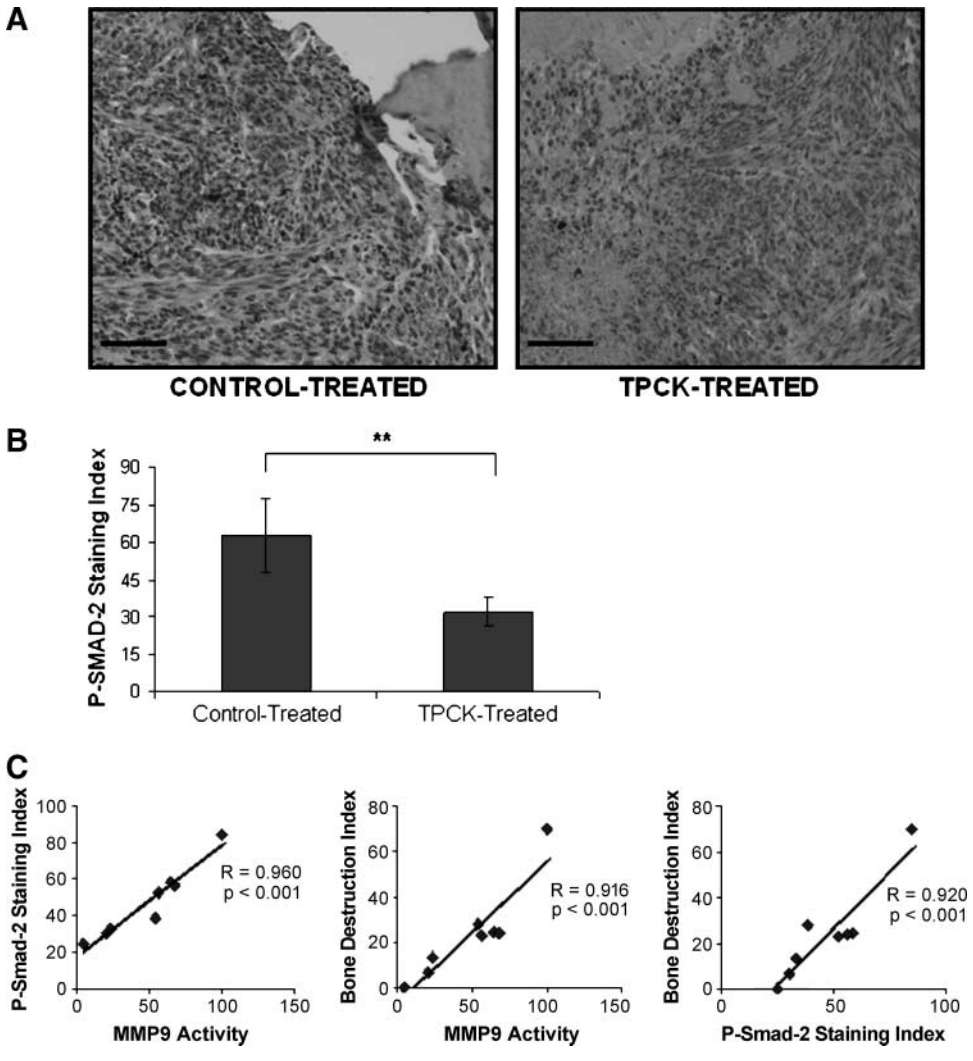

FIGURE 5. Inhibition of cathepsin G reduces TGF-β signaling at the tumor-bone interface. **A** and **B.** TPCK-treated mice showed a significantly reduced P-Smad-2 staining index at the tumor-bone interface compared with control (DMSO)–treated mice. Bars, SD. Scale bars, 0.01 mm. **, $P < 0.01$. **C.** Both MMP9 gelatinolytic activity at the tumor-bone interface and the P-Smad-2 staining index at the tumor-bone interface were positively correlated with the bone destruction index in TPCK- and control-treated mice. MMP9 activity was also positively correlated with the P-Smad-2 staining index.

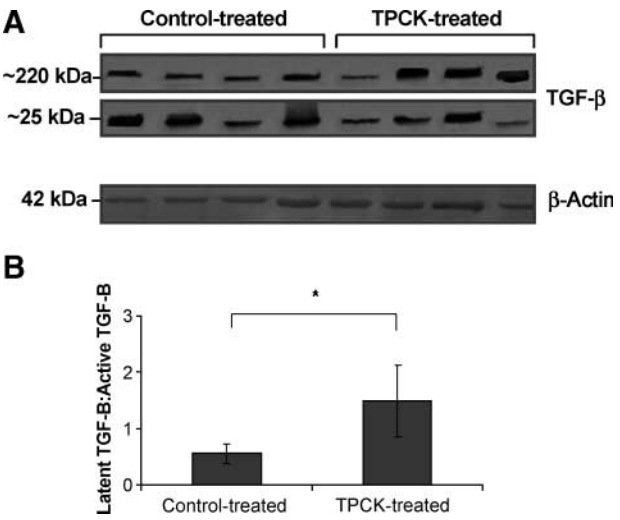

FIGURE 6. Inhibition of cathepsin G reduces active TGF-β at the tumor-bone interface. **A** and **B.** TPCK-treated animals showed a higher ratio of latent TGF-β (~220 kDa) to active TGF-β (~25 kDa) compared with control-treated animals. Bars, SD. *, $P < 0.05$.

adenocarcinoma cell line, mixed with growth factor–reduced Matrigel were implanted on the dorsal skin flap over the calvaria of female BALB/c mice ($n = 3$). Cl66 cells were used throughout this report based on previously reported up-regulation of cathepsin G and MMP9. However, similar observations were also made for Cl66M2 and 4T1 cells when used in the bone invasion model (3). Tumor growth was monitored twice a week. Mice were sacrificed and necropsied for examination of osteolytic lesions at 4 wk after implantation. At that time, the tumor and the underlying bone were divided into two pieces. One piece was used for separation of the tumor-bone interface from the tumor alone area for further analysis and the other piece was used for histology sections. All studies were done in accordance with the Institutional Animal Use and Care Committee of the University of Nebraska Medical Center. For histologic examination, tissues were fixed with periodate-lysine-paraformaldehyde at 4°C for 48 h. The tissues were then transferred into a decalcification solution (15% EDTA with glycerol, pH 7.4-7.5) for 4 wk. The tissue was then paraffin embedded and processed for further analysis.

Protein was extracted from the samples using T-PER tissue protein extractor solution (Pierce) following the manufacturer's provided protocol. Protein samples were quantified using a bicinchoninic acid protein assay kit (Pierce).

Immunohistochemistry for P-Smad-2

For *in vivo* evaluation of TGF-β signaling, we did immunohistochemistry for P-Smad-2 (20, 30-33). Sections were rehydrated using a series of xylenes and ethanols. Endogenous peroxidase activity was quenched using 3% H_2O_2 in methanol. Antigen retrieval was then done by boiling sections in 10 mmol/L sodium citrate buffer (pH 6.0) for 11 min. Sections were blocked using goat serum diluted 1:500 for 1 h at room temperature. Sections were then incubated overnight at 4°C with antibody directed against P-Smad-2 ($Ser^{465/467}$; Cell Signaling Technology) diluted 1:50 in blocking solution. After washing, sections were incubated for 1 h at room temperature with biotinylated anti-rabbit IgG diluted 1:500. After washing again, sections were incubated with avidin-biotin complex (Vectastain ABC, Vector Laboratories) for 45 min at room temperature. Sections were then washed and developed using diaminobenzidine tetrahydrochloride (Vector Laboratories) substrate. The sections were then counterstained with hematoxylin. Species-specific IgG isotype was added in lieu of primary antibody as a negative control, and these sections showed no detectable staining. For each section, ~8,000 nuclei were counted. The P-Smad-2 staining index was calculated by dividing the number of labeled nuclei by the total number of nuclei and multiplying by 100. The P-Smad-2 staining index was calculated for each section.

Gelatin Zymography

Total protein (50 μg) isolated from either the tumor-bone interface or tumor alone area from animals implanted with Cl66 tumors was subjected to electrophoresis on a 10% (w/v) polyacrylamide SDS gel containing 1 mg/mL porcine gelatin (Sigma-Aldrich). At the completion of electrophoresis, the gel was washed with 2.5% Triton X-100 buffer for 30 min. After rinsing, the gel was incubated for 12 h at 37°C in incubation buffer containing 50 mmol/L Tris-HCl (pH 7.4), 150 mmol/L NaCl, 10 mmol/L $CaCl_2$, and 0.05% (w/v) NaN_3. After rinsing, the gel was then stained using 0.025% Coomassie brilliant blue (Bio-Rad) and photographed using a MultiImage Light Cabinet (Alpha Innotech Corp.). The volume of gelatinolytic activity was evaluated using ImageQuant 5.1 (Molecular Dynamics).

sRANKL Treatment of Osteoclast Precursors

RAW 264.7 cells, a murine monocyte/macrophage cell line representing osteoclast precursors, were seeded onto 100-mm dishes at a density of 5,000/cm^2. They were allowed to incubate overnight. The next day, cells were treated with medium (DMEM plus 10% fetal bovine serum, 1% vitamins, 1% L-glutamine, and 0.08% gentamicin) plus 50 ng/mL sRANKL (Biomol International). RNA was collected from untreated RAW 264.7 cells and RAW 264.7 cells at 3, 5, and 7 d after sRANKL treatment for MMP9 mRNA analysis. Total RNA was isolated using Trizol reagent (Invitrogen). Total RNA (5 μg) was used for reverse transcription. First-strand cDNA was generated using oligo$(dT)_{18}$ (Fermentas) and SuperScript II RT (Invitrogen). The resulting cDNA (2 μL; 1:10 dilution) was used in the real-time reactions with gene-specific primers. Quantitative reverse transcription-PCRs (qRT-PCR) were carried out using FastStart SYBR Green Master mix (Roche) and a MyIQ iCycler (Bio-Rad). Fluorescence intensity was measured at the end of each elongation step as a means to evaluate the amount of formed PCR product. *GAPDH* was used as a reference to normalize the samples.

To assess gelatinolytic activity, cells were treated as described above in the absence of fetal bovine serum. Cell-free culture supernatants were collected and analyzed for MMP9 activity using gelatin zymography.

In vivo *RANKL Inhibition Using RANKL-ASOs*

ASOs used in the therapeutic protocol were obtained from Isis Pharmaceuticals. The ASOs used throughout this study were designed specific to RANKL. 2′-Methoxyethyl–modified

chimeric ASOs are synthesized as previously described (34). Active ASOs were identified by screening 46 ASOs designed to be specific for RANKL. These ASOs were transfected into cells and RNA was isolated 24 h later. RANKL mRNA levels were determined by RT-PCR, and the most effective ASOs were identified. The efficacy of these ASOs was confirmed in concentration-response experiments and the most potent ASO was used for further experiments. The RANKL-ASO sequence was 5′-GTCTTACACATGTATAGACA-3′. As a negative control, we used an oligonucleotide with the same chemical modifications but a sequence, 5′-TCTTATGTTTCC-GAACCGTT-3′, which did not match any known mRNA in the mouse genome. The oligonucleotides were dissolved in normal saline (0.9% NaCl) and administered by i.p. injection at a dose of 50 mg/kg/d starting at day 7 following tumor implantation for 5 d with 2 d off followed by another 4 d. Tumor growth was monitored and mice were sacrificed on day 28. Tumor alone and tumor-bone interface samples were collected and processed for gelatin zymography and P-Smad-2 immunostaining. Total RNA was isolated using Trizol reagent, and qRT-PCR was carried out as we previously described using gene-specific primers for *MMP2, MMP9*, and *GAPDH*.

Cathepsin G Activation of Pro-MMP9

Chromogenic MMP substrate (Biomol International) was incubated with 100 ng pro-MMP9 (Biomol International), 100 ng cathepsin G (Biomol International), or 100 ng pro-MMP9 preincubated with 200 ng cathepsin G for 6 h at 37°C in enough buffer to make a 50 μL reaction. The 10× buffer contained 100 mmol/L $CaCl_2$, 500 mmol/L HEPES, 10 mmol/L DTNB, and 0.5% Brij-35. The commercially available pro-MMP9 was primarily zymogen with some active form. Reaction mixtures were incubated at 37°C for 60 min. Absorbency was measured using a BioTek ELx800 microplate reader (BioTek) every 15 min at 405 nm.

Gelatin zymography was done as previously described using protein from the tumor alone area of control ASO–treated animals (where there is minimal MMP9 activity) and protein from the tumor alone area of control ASO–treated animals preincubated with cathepsin G for 2 h at 37°C.

In vivo *Inhibition of Cathepsin G Using TPCK*

Cathepsin G function was inhibited using TPCK in a murine bone invasion model as previously described (3). Cl66 tumor cells (1×10^5) mixed with growth factor–reduced Matrigel were implanted on the dorsal skin flap over the calvaria of female BALB/c mice. Tumor growth was monitored twice a week. Beginning 7 d after tumor implantation, mice were injected s.c. with TPCK (Sigma-Aldrich) at 50 mg/kg/d ($n = 4$) or 50 μL DMSO ($n = 4$) for 21 d. TPCK inhibits the chymotrypsin-like group of proteases and is a potent but nonspecific inhibitor of cathepsin G (35, 36). Mice were sacrificed at day 31 after implantation and necropsied for examination of osteolytic lesions. To calculate the bone destruction index, sections were stained with H&E. The bone destruction index was calculated by dividing the length of bone destruction by the length of the tumor-bone interface and multiplying by 100.

Gelatin zymography was done as previously described using protein from the tumor-bone interface of both TPCK- and control-treated mice. The percent of maximal gelatinolytic activity was calculated by dividing the volume of gelatinolytic activity of the given sample by the maximal volume for all of the samples and multiplying by 100.

Immunohistochemistry for P-Smad-2 to evaluate TGF-β signaling was done as previously described on sections from both TPCK- and control-treated mice.

Immunoblotting for TGF-β

Protein (75 μg) from the tumor-bone interface of control- and TPCK-treated mice was separated on a 12% polyacrylamide gel (nondenaturing) and then was transferred to a polyvinylidene difluoride membrane (GE Healthcare). The membranes were immunoblotted using 2 μg/mL anti–TGF-β antibody (R&D Systems) and 1:2,000 anti–β-actin antibody (Santa Cruz Biotechnology) and developed using an ECL Plus Western Blotting Detection System (GE Healthcare) per manufacturer's protocol and imaged using a Typhoon 9410 Variable Mode Imager (GE Healthcare). The bands for both TGF-β and β-actin were then quantified and compared using ImageQuant 5.1.

Statistical Analysis

For *in vitro* studies, the Student's *t* test was used for statistical comparison. For *in vivo* studies, the Mann-Whitney *U* test was used for statistical comparison. A P value of <0.05 was considered significant.

Disclosure of Potential Conflicts of Interest

No potential conflicts of interest were disclosed.

References

1. Jemal A, Siegel R, Ward E, et al. Cancer statistics, 2008. CA Cancer J Clin 2008;58:71–96.

2. Mundy GR. Metastasis to bone: causes, consequences and therapeutic opportunities. Nat Rev Cancer 2002;2:584–93.

3. Wilson TJ, Nannuru KC, Futakuchi M, Sadanandam A, Singh RK. Cathepsin G enhances mammary tumor-induced osteolysis by generating soluble receptor activator of nuclear factor-κB ligand. Cancer Res 2008;68:5803–11.

4. Lacey DL, Timms E, Tan HL, et al. Osteoprotegerin ligand is a cytokine that regulates osteoclast differentiation and activation. Cell 1998;93:165–76.

5. Dougall WC, Chaisson M. The RANK/RANKL/OPG triad in cancer-induced bone diseases. Cancer Metastasis Rev 2006;25:541–9.

6. Kitazawa S, Kitazawa R. RANK ligand is a prerequisite for cancer-associated osteolytic lesions. J Pathol 2002;198:228–36.

7. Roodman GD. Mechanisms of bone metastasis. N Engl J Med 2004;350:1655–64.

8. Zhang J, Dai J, Qi Y, et al. Osteoprotegerin inhibits prostate cancer-induced osteoclastogenesis and prevents prostate tumor growth in the bone. J Clin Invest 2001;107:1235–44.

9. Zhang J, Dai J, Yao Z, Lu Y, Dougall W, Keller ET. Soluble receptor activator of nuclear factor κB Fc diminishes prostate cancer progression in bone. Cancer Res 2003;63:7883–90.

10. Wilson TJ, Singh RK. Proteases as modulators of tumor-stromal interaction: primary tumors to bone metastases. Biochim Biophys Acta Rev Cancer 2008;1785:85–95.

11. Futakuchi M, Nannuru K, Varney ML, et al. Transforming growth factor-β signaling at the tumor-bone interface promotes mammary tumor growth and osteoclast activation. Cancer Sci 2009;100:71–81.

12. Yin JJ, Selander K, Chirgwin JM, et al. TGF-β signaling blockade inhibits PTHrP secretion by breast cancer cells and bone metastases development. J Clin Invest 1999;103:197–206.

13. Yu Q, Stamenkovic I. Cell surface-localized matrix metalloproteinase-9 proteolytically activates TGF-β and promotes tumor invasion and angiogenesis. Genes Dev 2000;14:163–76.

14. Olofsson A, Miyazono K, Kanzaki T, Colosetti P, Engstrom U, Heldin CH. Transforming growth factor-β1, -β2, and -β3 secreted by a human glioblastoma cell line. Identification of small and different forms of large latent complexes. J Biol Chem 1992;267:19482–8.

15. Koli K, Saharinen J, Hyytiainen M, Penttinen C, Keski-Oja J. Latency, activation, and binding proteins of TGF-β. Microsc Res Tech 2001;52:354–62.

16. Yoshinaga K, Obata H, Jurukovski V, et al. Perturbation of transforming growth factor (TGF)-β1 association with latent TGF-β binding protein yields inflammation and tumors. Proc Natl Acad Sci U S A 2008;105:18758–63.

17. Shamamian P, Schwartz JD, Pocock BJ, et al. Activation of progelatinase A (MMP-2) by neutrophil elastase, cathepsin G, and proteinase-3: a role for inflammatory cells in tumor invasion and angiogenesis. J Cell Physiol 2001; 189:197–206.

18. Sundaram K, Nishimura R, Senn J, Youssef RF, London SD, Reddy SV. RANK ligand signaling modulates the matrix metalloproteinase-9 gene expression during osteoclast differentiation. Exp Cell Res 2007;313:168–78.

19. Fujisaki K, Tanabe N, Suzuki N, et al. Receptor activator of NF-κB ligand induces the expression of carbonic anhydrase II, cathepsin K, and matrix metalloproteinase-9 in osteoclast precursor RAW264.7 cells. Life Sci 2007;80: 1311–8.

20. Nakao A, Imamura T, Souchelnytskyi S, et al. TGF-β receptor-mediated signalling through Smad2, Smad3 and Smad4. EMBO J 1997;16:5353–62.

21. Lynch CC, Hikosaka A, Acuff HB, et al. MMP-7 promotes prostate cancer-induced osteolysis via the solubilization of RANKL. Cancer Cell 2005;7:485–96.

22. Tanaka S. [A novel therapeutic vaccine approach against RANKL that prevents pathological bone destruction]. Clin Calcium 2005;15:62–6.

23. Gordon AH, O'Keefe RJ, Schwarz EM, Rosier RN, Puzas JE. Nuclear factor-κB-dependent mechanisms in breast cancer cells regulate tumor burden and osteolysis in bone. Cancer Res 2005;65:3209–17.

24. Morony S, Capparelli C, Sarosi I, Lacey DL, Dunstan CR, Kostenuik PJ. Osteoprotegerin inhibits osteolysis and decreases skeletal tumor burden in syngeneic and nude mouse models of experimental bone metastasis. Cancer Res 2001; 61:4432–6.

25. Tezuka K, Nemoto K, Tezuka Y, et al. Identification of matrix metalloproteinase 9 in rabbit osteoclasts. J Biol Chem 1994;269:15006–9.

26. Inui T, Ishibashi O, Origane Y, Fujimori K, Kokubo T, Nakajima M. Matrix metalloproteinases and lysosomal cysteine proteases in osteoclasts contribute to bone resorption through distinct modes of action. Biochem Biophys Res Commun 1999;258:173–8.

27. Okada Y, Naka K, Kawamura K, et al. Localization of matrix metalloproteinase 9 (92-kilodalton gelatinase/type IV collagenase = gelatinase B) in osteoclasts: implications for bone resorption. Lab Invest 1995;72:311–22.

28. Wucherpfennig AL, Li YP, Stetler-Stevenson WG, Rosenberg AE, Stashenko P. Expression of 92 kD type IV collagenase/gelatinase B in human osteoclasts. J Bone Miner Res 1994;9:549–56.

29. Reponen P, Sahlberg C, Munaut C, Thesleff I, Tryggvason K. High expression of 92-kDa type IV collagenase (gelatinase) in the osteoclast lineage during mouse development. Ann N Y Acad Sci 1994;732:472–5.

30. Massague J. TGF-β signal transduction. Annu Rev Biochem 1998;67: 753–91.

31. Heldin CH, Miyazono K, Ten DP. TGF-β signalling from cell membrane to nucleus through SMAD proteins. Nature 1997;390:465–71.

32. Miyazono K, Ten DP, Heldin CH. TGF-β signaling by Smad proteins. Adv Immunol 2000;75:115–57.

33. Lu Z, Murray JT, Luo W, et al. Transforming growth factor β activates Smad2 in the absence of receptor endocytosis. J Biol Chem 2002;277:29363–8.

34. Bennett CF, Cowsert LM. Antisense oligonucleotides as a tool for gene functionalization and target validation. Biochim Biophys Acta 1999;1489:19–30.

35. Overall CM, Blobel CP. In search of partners: linking extracellular proteases to substrates. Nat Rev Mol Cell Biol 2007;8:245–57.

36. Selak MA, Chignard M, Smith JB. Cathepsin G is a strong platelet agonist released by neutrophils. Biochem J 1988;251:293–9.